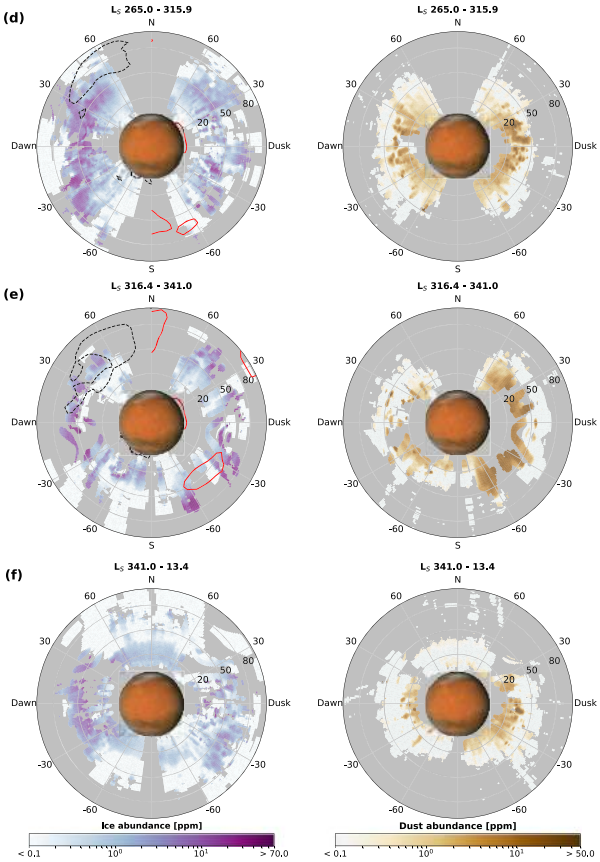

Figure 8. (continued)

atmospheric region, which is likely to occur as long as significant amounts of dust are in the middle atmosphere.

In the context of cloud formation processes, more interesting elements emerge from the comparison between the GDS and the January 2019 dust event. While there are numerous similarities between the spatial distributions of the mesospheric clouds that form during the peak of the two events, the average particle sizes are different (Figure 9). Limiting our comparison to the altitude range in which clouds form in both cases (40 to 80 km), we note that at all latitudes particle sizes are different, with values in the range 0.1–0.7 μm for the 2018 GDS and 0.1–2.0 μm in the January 2019 event. This significant difference is attributable to the differing water vapor abundance in the upper atmosphere during the two events. Indeed, because of the season and lower dust activity of the January 2019 with respect to the 2018 GDS, we effectively observe a lower water vapor abundance in the mesosphere during the January 2019 event, compared to the 2018 GDS, when water was observed at 80 km (Vandaele et al., 2019). The water profiles shown in Figure 9 are retrieved from NOMAD full resolution data, combining the retrievals from different diffraction orders (Aoki et al., 2019), and are the global averages of the profiles during the onset of the two storms. These phenomena are supported by Hartwick et al. (2019) that discuss the relation between the abundance of water vapor in the upper atmosphere and the availability of condensation nuclei. In this case, the 2019 dust event is characterized by less water vapor in the upper atmosphere than the GDS. Moreover, Figure 8 indicates that much less dust is available in the upper atmosphere in the 2019 event than during the GDS. The combination of these two leads to less competition in the condensation process, yielding to formation of larger ice particles (>1.0 μm), as observed during the 2019 dust event.

4. Discussion

4.1. Spatial and Temporal Distribution of Clouds

The results illustrated herein contribute to the discussion of atmospheric circulation and formation mechanisms for water ice clouds on Mars. Although a detailed comparison between our results and global circulation modeling is beyond the scope of this paper, we will make broad comparisons with the existing literature

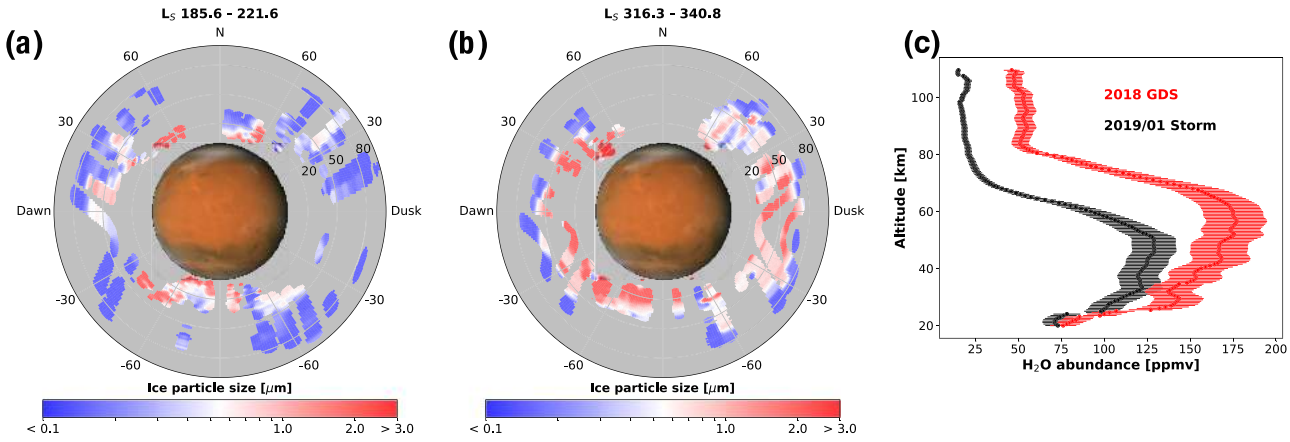

Figure 9. In the same format as Figure 8 we illustrate water ice particle sizes retrieved during the (left) GDS and (middle) January 2019 dust storm. On the right, the global averages of the water vapor vertical profiles retrieved from NOMAD data for the 2018 GDS (red) and the January 2019 storm (black).

on these topics. The latitudinal and temporal distribution of water ice clouds during the 2018 GDS (Figure 8) suggests a correlation between the enhancement of the water vapor circulation toward southern high latitudes during the GDS (seen in Neary et al., 2019) and the formation of high water ice clouds at high latitudes. Despite this, our results indicate that there are no significant differences in the ways that clouds are distributed at high latitudes in a global dust storm and non-GDS situation. The ideal reference for comparison are MCS retrievals (McCleese et al., 2010) during MY29. In both cases (McCleese et al., 2010, Figures 16 and 17), there is a clear break in the formation of high-altitude clouds in the NH, which occurs between midlatitudes (45 to 60°N; Figures 8b and 8c) and in the polar region. Clouds are seen only below 40 km both in MCS non-GDS retrievals and in this analysis.

Such comparisons show several differences for high-altitude water ice clouds. MCS results in the SH summer report that the top and the bottom levels of most clouds are roughly separated by 1 order of magnitude in pressure, which corresponds to more than two scale heights (25 to 30 km). As seen here though, the altitude distribution is frequently much more complex (Figures 5 and 8c), with clouds at the tropics and middle southern latitudes that extend for more than 40 km. The vertical extension is also subjected to dawn/dusk variations, which in the presence of a GDS are likely to occur, as discussed previously and suggested in other works (e.g., Smith, 2009). This depicts a complex cloud formation mechanism, which in the perihelion season considers both nucleation around dust and vertical and diurnal temperature gradients from the boundary layer through the mesosphere.

Comparison with MCS non-GDS retrievals also confirms that the rapid increase of cloud formation altitudes, seen in both the dust storms observed with NOMAD, is a storm-induced effect. Such a dramatic increase is not seen in MCS retrievals, as there is no tangible sign of a sudden variation of the vertical distribution of the clouds in the different time slots covered by MCS (L_S 180–225–270–315; McCleese et al., 2010, Figures 16 and 17). Low-altitude clouds presented in this work are in agreement with MCS retrievals between L_S 180 and 360. Both retrievals (GDS and non-GDS) cannot identify significant water ice extinction below 25 km around L_S 225, at nighttime for MCS and on the dawn terminator for NOMAD. The same agreement is found between daytime MCS retrievals and NOMAD at dusk, with significant differences only in the middle southern latitude toward L_S 270, where MCS found no significant amounts of water ice below 50 km. Such differences can also be explained by the enhancement of the downwelling branch of the meridional circulation during the GDS. No discrepancies are found between MCS and NOMAD retrievals at the equinox (L_S 0), where clouds form at decreasing altitudes as latitude increases. In this case, both retrievals show that at low latitudes water ice forms as low as 15 km at nighttime (dawn), while during the day the condensation altitude increases because of the solar heating, and clouds form only at 30 km.

4.2. Water Ice Particle Size: A Comparison With CRISM Retrievals

A great deal of information about the particle sizes of water ice in the atmosphere of Mars has been obtained by analyzing the limb data of the CRISM spectrometer. The present work increases the data coverage both in time and space with respect to CRISM, providing a more comprehensive assessment and validation of water ice particle sizes and their vertical and temporal variations.

The vertical structure found herein is consistent overall with the results presented in Clancy et al. (2019). Mesospheric water ice clouds exhibit a narrow range of particle sizes (0.1 to 0.3 μm); however, we have a larger number of cases where the retrieved average particle size is 0.1 μm (lower boundary imposed in the retrieval), as NOMAD retrievals are indicative of a particle size <0.1 μm. In the work of Clancy et al. (2019), there is a distinct decrease in detections for particles smaller than 0.1 μm, because smaller aerosols are difficult to discriminate against bigger particles in CRISM data, and can only appear as a continuum scattering component. While our results agree with the general conclusion that particle sizes decrease with increasing altitude, we detect a significant number of water ice clouds in the mesosphere, where the vertical structure of particle sizes is more complex. In such cases, particle sizes exhibit local maxima at the center of the cloud layer, and then decline rapidly toward the cloud top (Figure 9a). While it is difficult to track the spatial distribution of such cases, they appear more frequent in optically thick clouds characterized by the presence of one main layer, which form above 60 km. In any case, the water ice clouds presented in the CRISM study are typically discrete layers, presumably formed in the cold phase of gravity or tidal waves (Clancy et al., 2019), while NOMAD is frequently observing extended cloud hazes during the dust storm, which are situated below the bulk of mesospheric clouds.

Similar differences in complexity are seen in comparison with previous works (Guzewich et al., 2014; Guzewich & Smith, 2019) regarding water ice clouds in the lower atmosphere. In particular, Figure 6 (top) informs variations of water ice particle size in two different altitude ranges. Our lower atmospheric retrievals (10–40 km) show substantial disagreement with CRISM retrievals. Considering only those cases where retrieved water ice concentrations are significant, the average retrieved particle size (30°S–30°N; 20–40 km) is 2.7 μm at perihelion (L_S 240–260) and 2.2 μm at the equinoxes (L_S 170–190 and 350–10, MY35), in contrast to values, respectively, of 2.1 and 1.7 μm from CRISM. While the perihelion difference can be attributed to the dynamics related to the GDS, the discrepancy observed during the equinoxes is more difficult to explain, although it seems consistent with the sharp vertical gradients we see in particle sizes. Vertical variation of particle size appears to be much steeper than CRISM retrievals (Guzewich et al., 2014). On one hand, limb observations show greater sensitivity to characteristics otherwise difficult to constrain (i.e., particle phase function, shape) so the difference between retrievals might not be really significant. On the other hand, there is the possibility that water saturation is sufficiently high or low that particle growth is more or less efficient than expected. This aspect deserves to be further investigated by dedicated modeling work.

In general, the frequent detection of mesospheric water ice clouds composed of small particles poses some interesting questions related to their impact on the radiative balance in the upper atmosphere, and the lower altitude layers. Previous works (e.g., Madeleine et al., 2011) have already shown the presence of a permanent cold bias around 0.1 mbar, which can be mainly attributed to the exclusion of the radiative effects of high-altitude water ice clouds composed by small particles, especially during the perihelion. In fact, this population of clouds cannot be captured by the unimodal size distribution assumed in dust transport models included in some GCMs. This modeling limitation has been questioned recently in Hartwick et al. (2019), where it is shown how a model including meteoric smoke can account for such observations. The retrievals we have presented here do not provide a final word on nucleation processes in the upper atmosphere, since the thermal information is not fully integrated into this analysis. However, the dawn/dusk NOMAD measurements can certainly inform on those processes in a complementary fashion to the MCS 3 am/3 pm retrievals, which have been used as a benchmark in the work by *Hartwick et al.* In addition, the capability of NOMAD observations to extensively constrain water ice and dust abundance and properties up to 100 km is of great importance in this context. The present work is only the most recent showing the persistent presence of such clouds at many latitudes.

5. Conclusions

NOMAD measurements contain a breadth of information on Martian atmospheric aerosols. By using all the available data taken by NOMAD in Solar Occultation, we have retrieved vertical profiles of water ice, dust, and their particle sizes, with a resolution around 1 km, a maximum vertical sampling of 600 m, from the lower atmosphere to 110 km. To accomplish this, we have developed a robust retrieval methodology to treat NOMAD SO broadband data. Given the number of available points, this is an underconstrained problem, the resolution of which constitutes an important piece of work. We have generally obtained robust results, characterized the errors and the information content, highlighting the consistency of retrieved water ice properties, and the caveats associated to the dust retrievals. In general, these results indicate that when the observed transmittance is above 1%, retrievals are robust enough to separate water ice from dust, and quantify their microphysical properties.

We have analyzed NOMAD data from April 2018 to April 2019, for a total of 1,781 profiles. This period encompasses the 2018 GDS, which was observed to have tremendous effects not only on the vertical distribution of water vapor, as shown in previous studies, but also on water ice cloud formation. The rapid lifting of the water ice condensation altitude is a peculiarity of dust storms, since it has not been observed in a non-GDS situation previously. This effect has been seen to last for a long period (80° L_S) after the onset of the storm. Clouds are observed as high as 90 km at the beginning of the GDS, while dust elevates up to 70 km.

Water ice clouds have been observed at dawn and dusk. There are remarkable differences between the two, with optically thicker (larger concentrations) mesospheric clouds at dawn than dusk due to nighttime condensation of water vapor. The combination of dust and ice observations between dawn and dusk reveals how

dust grains are subjected to nighttime scavenging by water ice. Observations suggest that this process decreases in intensity as the GDS dissipates. Dawn versus dusk analysis also reveals the presence of dusk high-latitude mesospheric clouds in the SH during the most intense phase of the GDS, which is compatible with a strong enhancement of the downwelling branch of the meridional circulation.

We characterized the particle sizes of mesospheric water ice clouds with a precision around 0.1 μm. The majority of water ice cloud particle size vertical profiles exhibit sharp vertical gradients. Specifically, mesospheric water ice particles have sizes between 0.1 and 0.5 μm, which decrease with altitude. However, the comparison with literature shows previously undetected complexities in the vertical profiles of water ice and particle sizes, which constitute exceptions to this general trend. Retrievals have shown significant discrepancies between particle sizes of mesospheric clouds during the GDS and those during the January 2019 dust event. We have attributed this difference to the larger availability of H_2O and dust in the mesosphere during the GDS than the 2019 event, which results in differing condensation efficiencies.

These elements, together with the observed large vertical and temporal variability of water ice particle size, pose questions about the description of water ice nucleation processes into models. In particular, the accuracy of NOMAD retrievals of water ice in the mesosphere up to 100 km constitute a precious source to validate current working hypotheses on the role of both planetary and interplanetary dust as condensation nuclei at various altitudes. Furthermore, the observations we have presented are important to fill in the existing temporal gaps in the literature, and can serve as a database to be assimilated into global circulation models, going beyond the simple elaboration of climatology for these quantities.

Acknowledgments
ExoMars is a space mission of the European Space Agency (ESA) and Roscosmos. The NOMAD experiment is led by the Royal Belgian Institute for Space Aeronomy (IASB-BIRA), assisted by Co-PI teams from Spain (IAA-CSIC), Italy (INAF-IAPS), and the United Kingdom (Open University). This project acknowledges funding by the Belgian Science Policy Office (BELSPO), with the financial and contractual coordination by the ESA Prodex Office (PEA 4000103401, 4000121493), by the Spanish MICINN through its Plan Nacional and by European funds under grants PGC2018-101836-B-I00 and ESP2017-87143-R (MINECO/FEDER), and by UK Space Agency through grants ST/R005761/1, ST/P001262/1, ST/R001405/1, and ST/S00145X/1 and Italian Space Agency through grant 2018-2-HH.0. The IAA/CSIC team acknowledges financial support from the State Agency for Research of the Spanish MCIU through the "Center of Excellence Severo Ochoa" award for the Instituto de Astrofísica de Andalucía (SEV-2017-0709). This work was supported by NASA's Mars Program Office under WBS 604796, "Participation in the TGO/NOMAD Investigation of Trace Gases on Mars" and by NASA's SEEC initiative under grant NNX17AH81A, "Remote sensing of Planetary Atmospheres in the Solar System and Beyond." M.C. is supported by the NASA Postdoctoral Program at the NASA Goddard Space Flight Center, administered by Universities Space Research Association (USRA) under contract with NASA. The retrieval package used in this study is the Planetary Spectrum Generator, free and available online at https://psg.gsfc.nasa.gov/helpatm.php#retrieval, at the PSG GitHub site: https://github.com/nasapsg/retrievalOE, and on Zenodo (Liuzzi, 2020a). The database with the retrieved values is available of the PSG Exomars server at https://psg.gsfc.nasa.gov/apps/exomars.php and on Zenodo (Liuzzi, 2020b). The data used in this analysis are available at https://nomad.aeronomie.be/index.php/data.

References

Aoki, S., Vandaele, A. C., Daerden, F., Villanueva, G., Liuzzi, G., Thomas, I. R., et al., & the NOMAD team (2019). Water vapor vertical profiles on Mars in dust storms observed by TGO/NOMAD. *Journal of Geophysical Research: Planets*, *124*, 3482–3497. https://doi.org/10.1029/2019JE006109

Bertaux, J.-L., Korablev, O., Perrier, S., Quémerais, E., Montmessin, F., Leblanc, F., et al. (2006). SPICAM on Mars Express: Observing modes and overview of UV spectrometer data and scientific results. *Journal of Geophysical Research*, *111*, E10S90. https://doi.org/10.1029/2006JE002690

Carissimo, A., De Feis, I., & Serio, C. (2005). The physical retrieval methodology for IASI: The δ-IASI code. *Environmental Modelling & Software*, *20*(9), 1111–1126. https://doi.org/10.1016/j.envsoft.2004.07.003

Christensen, P. R., Bandfield, J. L., Hamilton, V. E., Ruff, S. W., Kieffer, H. H., Titus, T. N., et al. (2001). Mars Global Surveyor Thermal Emission Spectrometer experiment: Investigation description and surface science results. *Journal of Geophysical Research*, *106*(E10), 2,3823–23,871. https://doi.org/10.1029/2000JE001370

Clancy, R. T., Wolff, M. J., & Christensen, P. R. (2003). Mars aerosol studies with the MGS TES emission phase function observations: Optical depths, particle sizes, and ice cloud types versus latitude and solar longitude. *Journal of Geophysical Research*, *108*(E9), 5098. https://doi.org/10.1029/2003JE002058

Clancy, R. T., Wolff, M. J., Smith, M. D., Kleinböhl, A., Cantor, B. A., Murchie, S. L., et al. (2019). The distribution, composition, and particle properties of Mars mesospheric aerosols: An analysis of CRISM visible/near-IR limb spectra with context from near-coincident MCS and MARCI observations. *Icarus*, *328*, 246–273. https://doi.org/10.1016/j.icarus.2019.03.025

Clancy, R. T., Grossman, A. W., Wolff, M. J., James, P. B., Rudy, D. J., Billawala, Y. N., et al. (1996). Water vapor saturation at low altitudes around Mars aphelion: A key to Mars climate? *Icarus*, *122*(1), 36–62. https://doi.org/10.1006/icar.1996.0108

Clancy, R. T., Sandor, B. J., Wolff, M. J., Christensen, P. R., Smith, M. D., Pearl, J. C., et al. (2000). An intercomparison of ground-based millimeter, MGS TES, and Viking atmospheric temperature measurements: Seasonal and interannual variability of temperatures and dust loading in the global Mars atmosphere. *Journal of Geophysical Research*, *105*(E4), 9553–9571. https://doi.org/10.1029/1999JE001089

Crismani, M. M. J., Schneider, N. M., Plane, J. M. C., Evans, J. S., Jain, S. K., Chaffin, M. S., et al. (2017). Detection of a persistent meteoric metal layer in the Martian atmosphere. *Nature Geoscience*, *10*(6), 401–404. https://doi.org/10.1038/ngeo2958

Fedorova, A., Bertaux, J.-L., Betsis, D., Montmessin, F., Korablev, O., Maltagliati, L., & Clarke, J. (2018). Water vapor in the middle atmosphere of Mars during the 2007 global dust storm. *Icarus*, *300*, 440–457. https://doi.org/10.1016/j.icarus.2017.09.025

Fedorova, A. A., Montmessin, F., Rodin, A. V., Korablev, O. I., Määttänen, A., Maltagliati, L., & Bertaux, J.-L. (2014). Evidence for a bimodal size distribution for the suspended aerosol particles on Mars. *Icarus*, *231*, 239–260. https://doi.org/10.1016/j.icarus.2013.12.015

Gurwell, M. A., Bergin, E. A., Melnick, G. J., & Tolls, V. (2005). Mars surface and atmospheric temperature during the 2001 global dust storm. *Icarus*, *175*(1), 23–31. https://doi.org/10.1016/j.icarus.2004.10.009

Guzewich, S. D., Lemmon, M., Smith, C. L., Martínez, G., de Vicente-Retortillo, Á., Newman, C. E., et al. (2019). Mars Science Laboratory observations of the 2018/Mars year 34 global dust storm. *Geophysical Research Letters*, *46*, 71–79. https://doi.org/10.1029/2018GL080839

Guzewich, S. D., & Smith, M. D. (2019). Seasonal variation in Martian water ice cloud particle size. *Journal of Geophysical Research: Planets*, *124*, 636–643. https://doi.org/10.1029/2018JE005843

Guzewich, S. D., Smith, M. D., & Wolff, M. J. (2014). The vertical distribution of Martian aerosol particle size. *Journal of Geophysical Research: Planets*, *119*, 2694–2708. https://doi.org/10.1002/2014JE004704

Guzewich, S. D., Talaat, E. R., Toigo, A. D., Waugh, D. W., & McConnochie, T. H. (2013). High-altitude dust layers on Mars: Observations with the Thermal Emission Spectrometer. *Journal of Geophysical Research: Planets*, *118*, 1177–1194. https://doi.org/10.1002/jgre.20076

Haberle, R., Clancy, R. T., Forget, F., Smith, M. D., & Zurek, R. (2017). The atmosphere and climate of mars. https://10.1017/9781139060172

Hartwick, V. L., Toon, O. B., & Heavens, N. G. (2019). High-altitude water ice cloud formation on Mars controlled by interplanetary dust particles. *Nature Geoscience*, *12*(7), 516–521. https://doi.org/10.1038/s41561-019-0379-6

Heavens, N. G., Richardson, M. I., Kleinböhl, A., Kass, D. M., McCleese, D. J., Abdou, W., et al. (2011). The vertical distribution of dust in the Martian atmosphere during northern spring and summer: Observations by the Mars Climate Sounder and analysis of zonal average vertical dust profiles. *Journal of Geophysical Research*, *116*, E04003. https://doi.org/10.1029/2010JE003691

Heavens, N. G., Kass, D. M., & Shirley, J. H. (2019). Dusty deep convection in the Mars year 34 planet-encircling dust event. *Journal of Geophysical Research: Planets*, *124*, 2863–2892. https://doi.org/10.1029/2019JE006110

Heavens, N. G., Kleinböhl, A., Chaffin, M. S., Halekas, J. S., Kass, D. M., Hayne, P. O., et al. (2018). Hydrogen escape from Mars enhanced by deep convection in dust storms. *Nature Astronomy*, *2*(2), 126–132. https://doi.org/10.1038/s41550-017-0353-4

Kahre, M. A., Hollingsworth, J. L., Haberle, R. M., & Murphy, J. R. (2008). Investigations of the variability of dust particle sizes in the Martian atmosphere using the NASA Ames general circulation model. *Icarus*, *195*(2), 576–597. https://doi.org/10.1016/j.icarus.2008.01.023

Kass, D. M., Kleinböhl, A., McCleese, D. J., Schofield, J. T., & Smith, M. D. (2016). Interannual similarity in the Martian atmosphere during the dust storm season. *Geophysical Research Letters*, *43*, 6111–6118. https://10.1002/2016GL068978 Kleinböhl, A., Schofield, J. T., Kass, D. M., Abdou, W. A., Backus, C. R., Sen, B., et al. (2009). Mars Climate Sounder limb profile retrieval of atmospheric temperature, pressure, and dust and water ice opacity. *Journal of Geophysical Research*, *114*, E10006. https://doi.org/10.1029/2009JE003358

Korablev, O., Montmessin, F., Trokhimovskiy, A., Fedorova, A. A., Shakun, A. V., Grigoriev, A. V., et al. (2017). The Atmospheric Chemistry Suite (ACS) of three spectrometers for the ExoMars 2016 Trace Gas Orbiter. *Space Science Reviews*, *214*(1), 1–62. https://doi.org/10.1007/s11214-017-0437-6

Lee, C., Lawson, W. G., Richardson, M. I., Heavens, N. G., Kleinböhl, A., Banfield, D., et al. (2009). Thermal tides in the Martian middle atmosphere as seen by the Mars Climate Sounder. *Journal of Geophysical Research*, *114*, E03005. https://doi.org/10.1029/2008JE003285

Liuzzi, G. (2020a). Retrieval code in support of the publication "Strong variability of Martian water ice clouds during dust storms revealed from ExoMars Trace Gas Orbiter/NOMAD" on JGR-Planets, https://doi.org/10.5281/zenodo.3691975

Liuzzi, G. (2020b). Data in support of manuscript submitted to JGR-Planets "Strong variability of Martian water ice clouds during dust storms revealed from ExoMars Trace Gas Orbiter/NOMAD", https://doi.org/10.5281/zenodo.3637564

Liuzzi, G., Masiello, G., Serio, C., Venafra, S., & Camy-Peyret, C. (2016). Physical inversion of the full IASI spectra: Assessment of atmospheric parameters retrievals, consistency of spectroscopy and forward modelling. *Journal of Quantitative Spectroscopy and Radiative Transfer*, *182*, 128–157. https://doi.org/10.1016/j.jqsrt.2016.05.022

Liuzzi, G., Villanueva, G. L., Mumma, M. J., Smith, M. D., Daerden, F., Ristic, B., et al. (2019). Methane on Mars: New insights into the sensitivity of CH_4 with the NOMAD/ExoMars spectrometer through its first in-flight calibration. *Icarus*, *321*, 671–690. https://doi.org/10.1016/j.icarus.2018.09.021

Luginin, M., Fedorova, A., Ignatiev, N., Grigoriev, A., Trokhimovskiy, A., Shakun, A., et al. (2019). One year of observations of dust and water ice aerosols performed by ACS TIRVIM and NIR, European Planetary Science Congress/Division of Planetary Science, EPSC-DPS2019–1316-1.

Määttänen, A., Listowski, C., Montmessin, F., Maltagliati, L., Reberac, A., Joly, L., & Bertaux, J.-L. (2013). A complete climatology of the aerosol vertical distribution on Mars from MEx/SPICAM UV solar occultations. *Icarus*, *223*(2), 892–941. https://doi.org/10.1016/j.icarus.2012.12.001

Madeleine, J.-B., Forget, F., Millour, E., Montabone, L., & Wolff, M. J. (2011). Revisiting the radiative impact of dust on Mars using the LMD global climate model. *Journal of Geophysical Research*, *116*, E11010. https://doi.org/10.1029/2011JE003855

Mahieux, A., Berkenbosch, S., Clairquin, R., Fussen, D., Mateshvili, N., Neefs, E., et al. (2008). In-flight performance and calibration of SPICAV SOIR onboard Venus Express. *Applied Optics*, *47*(13), 2252–2265. https://doi.org/10.1364/ao.47.002252

McCleese, D. J., Heavens, N. G., Schofield, J. T., Abdou, W. A., Bandfield, J. L., Calcutt, S. B., et al. (2010). Structure and dynamics of the Martian lower and middle atmosphere as observed by the Mars Climate Sounder: Seasonal variations in zonal mean temperature, dust, and water ice aerosols. *Journal of Geophysical Research*, *115*, E12016. https://doi.org/10.1029/2010JE003677

McCleese, D. J., Schofield, J. T., Taylor, F. W., Calcutt, S. B., Foote, M. C., Kass, D. M., et al. (2007). Mars Climate Sounder: An investigation of thermal and water vapor structure, dust and condensate distributions in the atmosphere, and energy balance of the polar regions. *Journal of Geophysical Research*, *112*, E05S06. https://doi.org/10.1029/2006JE002790

Michelangeli, D. V., Toon, O. B., Haberle, R. M., & Pollack, J. B. (1993). Numerical simulations of the formation and evolution of water ice clouds in the Martian atmosphere. *Icarus*, *102*(2), 261–285. https://doi.org/10.1006/icar.1993.1048

Millour, E., Forget, F., Spiga, A., Navarro, T., Madeleine, J.-B., Montabone, L., et al., and the MCD/GCM development team (2015). The Mars Climate Database (MCD version 5.2). *European Planetary Science Congress*, *10*, EPSC2015-438.

Montabone, L., Forget, F., Millour, E., Wilson, R. J., Lewis, S. R., Cantor, B., et al. (2015). Eight-year climatology of dust optical depth on Mars. *Icarus*, *251*, 65–95. https://doi.org/10.1016/j.icarus.2014.12.034

Montmessin, F., Korablev, O., Lefèvre, F., Bertaux, J.-L., Fedorova, A., Trokhimovskiy, A., et al. (2017). SPICAM on Mars Express: A 10 year in-depth survey of the Martian atmosphere. *Icarus*, *297*, 195–216. https://doi.org/10.1016/j.icarus.2017.06.022

Murchie, S., Arvidson, R., Bedini, P., Beisser, K., Bibring, J.-P., Bishop, J., et al. (2007). Compact Reconnaissance Imaging Spectrometer for Mars (CRISM) on Mars Reconnaissance Orbiter (MRO). *Journal of Geophysical Research*, *112*, E05S03. https://doi.org/10.1029/2006JE002682

Navarro, T., Madeleine, J.-B., Forget, F., Spiga, A., Millour, E., Montmessin, F., & Määttänen, A. (2014). Global climate modeling of the Martian water cycle with improved microphysics and radiatively active water ice clouds. *Journal of Geophysical Research: Planets*, *119*, 1479–1495. https://doi.org/10.1002/2013JE004550

Neary, L., Daerden, F., Aoki, S., Whiteway, J., Clancy, R. T., Smith, M., et al. (2019). Explanation for the increase in high altitude water on Mars observed by NOMAD during the 2018 global dust storm. *Geophysical Research Letters*, *46*. https://doi.org/10.1029/2019GL084354

Neefs, E., Vandaele, A. C., Drummond, R., Thomas, I. R., Berkenbosch, S., Clairquin, R., et al. (2015). NOMAD spectrometer on the ExoMars Trace Gas Orbiter mission: Part 1—Design, manufacturing and testing of the infrared channels. *Applied Optics*, *54*(28), 8494–8520. https://doi.org/10.1364/AO.54.008494

Nevejans, D., Neefs, E., Van Ransbeeck, E., Berkenbosch, S., Clairquin, R., De Vos, L., et al. (2006). Compact high-resolution spaceborne echelle grating spectrometer with acousto-optical tunable filter based order sorting for the infrared domain from 2.2 to 4.3 μm. *Applied Optics*, *45*(21), 5191–5206. https://doi.org/10.1364/ao.45.005191

Plane, J. M. C., Carrillo-Sanchez, J. D., Mangan, T. P., Crismani, M. M. J., Schneider, N. M., & Määttänen, A. (2018). Meteoric metal chemistry in the Martian atmosphere. *Journal of Geophysical Research: Planets*, *123*, 695–707. https://doi.org/10.1002/2017JE005510

Rodgers, C. D. (2000). Inverse methods for atmospheric sounding, *Series on atmospheric*, *Oceanic and Planetary Physics*, *2*. https://www.worldscientific.com/worldscibooks/, https://doi.org/10.1142/3171

Rodin, A. V., Clancy, R. T., & Wilson, R. J. (1999). Dynamical properties of Mars water ice clouds and their interactions with atmospheric dust and radiation. *Advances in Space Research*, *23*(9), 1577–1585. https://doi.org/10.1016/S0273-1177(99)00173-8

Sefton-Nash, E., Teanby, N. A., Montabone, L., Irwin, P. G. J., Hurley, J., & Calcutt, S. B. (2013). Climatology and first-order composition estimates of mesospheric clouds from Mars Climate Sounder limb spectra. *Icarus*, *222*(1), 342–356. https://doi.org/10.1016/j.icarus.2012.11.012

Slipski, M., Jakosky, B. M., Benna, M., Elrod, M., Mahaffy, P., Kass, D., et al. (2018). Variability of Martian turbopause altitudes. *Journal of Geophysical Research: Planets*, *123*, 2939–2957. https://doi.org/10.1029/2018JE005704

Smith, M. D. (2004). Interannual variability in TES atmospheric observations of Mars during 1999–2003. *Icarus*, *167*(1), 148–165. https://doi.org/10.1016/j.icarus.2003.09.010

Smith, M. D. (2008). Spacecraft observations of the Martian atmosphere. *Annual Review of Earth and Planetary Sciences*, *36*(1), 191–219. https://doi.org/10.1146/annurev.earth.36.031207.124334

Smith, M. D. (2009). THEMIS observations of Mars aerosol optical depth from 2002–2008. *Icarus*, *202*(2), 444–452. https://doi.org/10.1016/j.icarus.2009.03.027

Smith, M. D., Wolff, M. J., Clancy, R. T., Kleinböhl, A., & Murchie, S. L. (2013). Vertical distribution of dust and water ice aerosols from CRISM limb-geometry observations. *Journal of Geophysical Research: Planets*, *118*, 321–334. https://doi.org/10.1002/jgre.20047

Spiga, A., Faure, J., Madeleine, J.-B., Määttänen, A., & Forget, F. (2013). Rocket dust storms and detached dust layers in the Martian atmosphere. *Journal of Geophysical Research: Planets*, *118*, 746–767. https://doi.org/10.1002/jgre.20046

Stamnes, K., Thomas, G. E., & Stamnes, J. J. (2017). *Radiative transfer in the atmosphere and ocean*. Cambridge: Cambridge University Press. https://doi.org/10.1017/9781316148549

Thomas, I. R., Vandaele, A. C., Robert, S., Neefs, E., Drummond, R., Daerden, F., et al., & NOMAD Team (2016). Optical and radiometric models of the NOMAD instrument: Part II—The infrared channels—SO and LNO. *Optics Express*, *24*(4), 3790–3805. https://doi.org/10.1364/OE.24.003790

Vandaele, A. C., Lopez-Moreno, J.-J., Patel, M. R., Bellucci, G., Daerden, F., Ristic, B., et al. (2018). NOMAD, an integrated suite of three spectrometers for the ExoMars Trace Gas mission: Technical description, science objectives and expected performance. *Space Science Reviews*, *214*(5), 1–47. https://doi.org/10.1007/s11214-018-0517-2

Vandaele, A. C., Neefs, E., Drummond, R., Thomas, I. R., Daerden, F., Lopez-Moreno, J.-J., et al. (2015). Science objectives and performances of NOMAD, a spectrometer suite for the ExoMars TGO mission. *Planetary and Space Science*, *119*, 233–249. https://doi.org/10.1016/j.pss.2015.10.003

Vandaele, Ann Carine, Korablev, O., Daerden, F., Aoki, S., Thomas, I. R., Altieri, F., Miguel López-et al. (2019). Martian dust storm impact on atmospheric H_2O and D/H observed by ExoMars Trace Gas Orbiter. *Nature*, *568*. https://doi.org/10.1038/s41586-019-1097-3, 7753, 521–525

Villanueva, G. L., Smith, M. D., Protopapa, S., Faggi, S., & Mandell, A. M. (2018). Planetary spectrum generator: An accurate online radiative transfer suite for atmospheres, comets, small bodies and exoplanets. *Journal of Quantitative Spectroscopy and Radiative Transfer*, *217*, 86–104. https://doi.org/10.1016/j.jqsrt.2018.05.023

Warren, S. G., & Brandt, R. E. (2008). Optical constants of ice from the ultraviolet to the microwave: A revised compilation. *Journal of Geophysical Research*, *113*, D14220. https://doi.org/10.1029/2007JD009744

Whiteway, J. A., Komguem, L., Dickinson, C., Cook, C., Illnicki, M., Seabrook, J., et al. (2009). Mars water-ice clouds and precipitation. *Science*, *325*(5936), 68–70. https://doi.org/10.1126/science.1172344

Wolff, M. J., Smith, M. D., Clancy, R. T., Arvidson, R., Kahre, M., Seelos, F., et al. (2009). Wavelength dependence of dust aerosol single scattering albedo as observed by the Compact Reconnaissance Imaging Spectrometer. *Journal of Geophysical Research*, *114*, E00D04. https://doi.org/10.1029/2009JE003350